BENIN JOURNAL OF PHYSICAL SCIENCES
BJPS Vol. 2(1), June, pg. 175-192 (2025)
ISSN 3043-6931(Print)
3043-694X(Online)
www.bjps.org.ng

Characteristics of Dimensionless Pressures and Derivatives of a Horizontal Well Completed Within Oil Reservoir Sealing Boundaries Inclined at 45 Degrees

S. E. ASUQUO[1] and E. S. ADEWOLE[2,*]

[1]*Department of Petroleum Engineering, University of Calabar, Nigeria*
[2]*Department of Petroleum Engineering, University of Benin, BeninCity, Nigeria*

Received: 03/06/2025 ***Accepted:*** 29/06/2025

Abstract

This paper investigates dimensionless pressure and derivative distributions of a horizontal well completed within an oil reservoir with sealing external boundaries inclined at 45°. The total dimensionless pressure of an object horizontal well, based on its distance from the boundaries, well design, wellbore storage and skin, was derived by superposition principle accounting for all image wells generated due to inclination of the boundaries of the reservoir. Infinite-acting flow period was assumed to prevail throughout flow. The results indicate that there are seven (7) image wells generated due to the inclination. Dimensionless pressure gradients and derivatives of 9.2104/L_D and 4/L_D, respectively, characterized flow at large dimensionless flow times. Higher dimensionless well length prolonged the pseudo-linear flow regime, delaying boundary-dominated flow. Larger dimensionless well radii increased early-time pressure gradients. High skin factors and wellbore storage caused increased pressure drop and delayed response of transients by the inclined reservoir external boundaries. The farther the horizontal well from the external boundaries, the longer the well experienced infinite-acting flow, and therefore, delayed pseudosteady state flow. The study can provide a guide on horizontal well location and completion that can assist in optimizing oil recovery in reservoirs with sealing boundaries inclined at 45 degrees.

Keywords: *Horizontal Well, Sealing Boundary, Inclination*

*Corresponding author e-mail:steve.adewole@uniben.edu

1. INTRODUCTION

Horizontal wells offer numerous benefits, like enhancing hydrocarbon production by increasing reservoir contact and improving drainage efficiency compared to vertical wells. However, when the well is completed within sealing and inclined boundaries, well location has to be decided for optimum recovery. Chiefly, the well location has to be decided as a function of the inclination and distance from the inclined sealing boundaries. This study extends previous and similar researches by investigating the influence of sealing boundaries with inclination of 45 degrees on pressure and derivative responses. Figure 1 shows a schematic of a horizontal well completed within a pair of sealing boundaries inclined at 45 degrees.

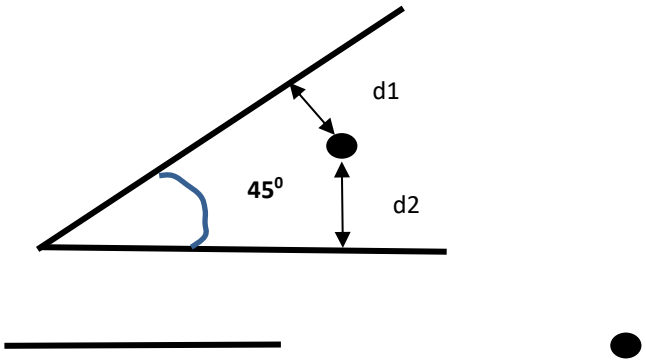

Figure 1: *Horizontal Well within a Pair of Sealing Boundaries Inclined at 45 Degrees*

Early authors of the subject of reservoir system characterization have discussed horizontal well flow in detail (Kuchuk(1995), Odeh et al(1990), Escobar et al(2004)). Earlougher(1977) showed that, vertical wellbore flowing pressure relationship exhibits a doubling of slope against log of flow time, if it is completed near a sealing boundary. Babu et al(1990) discussed pressure buildup and drawdown test analysis of infinite-acting horizontal wells. Ozkan et al(1990) investigated horizontal well behaviour when completed in a laterally infinite reservoir subject to bottom water drive. But Galas et al(1994) investigated the performance of horizontal wells in an enhanced oil recovery project. Daviau et al(1988) performed detailed analysis of horizontal well test based on pressure distribution using source and Green's functions. Successes in transient pressure analysis were led by Carslaw et al(1959), who considered heat conduction through solids as analogous to oil and gas wells flow. Matthews et al(1967) and Gringarten et al(1973) discussed transient pressure computations involving the exponential integral function and identified flow periods in wells. In all these cases, boundary inclination and type were not considered . However, Al Rbeawi et al(2013) discussed test analysis for horizontal wells completed within a multi-boundary

reservoir system. This study will fill an existing gap by developing a model that captures the pressure behavior of a horizontal well within sealing boundaries inclined at 45 degrees in particular, incorporating well design, near wellbore problems, like wellbore storage and skin factor.

2. MATERIALS AND METHOD

To obtain an accurate pressure drop expression, these facts about the inclined sealing boundaries have to be established: The boundaries behave like plane mirrors. The boundaries, therefore, form images of objects. As physical boundaries (barriers) they receive transients (stream energy) and reflect the stream energy (produce echoes). The images formed also produce echoes, which reduce the intensity of the streamlines. Therefore, the strength of transient in a well, that is, pressure drop in a well, depends on the number and distance of the image wells from the object well.

2.1 Image Well Location Procedure

To obtain the number and distances of the image wells, the following steps were followed:

1. Produced a polygon of side $360^0/45^0 = 8$ sides
2. Located the object well within one of the sectors of the polygon, at several dimensionless distances of d1, from the upper boundary and several dimensionless distances of d2, from the lower boundary.
3. From the center of the object well, we produced a line, length, d1, to hit the top mirror (sealing boundary) a right angle.
4. We located the first image at a distance equal to D1, in a counterclockwise direction.
5. This image was now an object to the next mirror. We produced a line to hit the next mirror a right angle. We measured the distance from the next mirror, and also measured the new image distance from the new mirror.
6. The procedure was continued as in Step 5 until the image produced 'saw' the object well. The new images served as objects to every new mirror. A polygon was produced in the end. If the object well distances from top and bottom mirrors were the same, then the polygon produced was a regular polygon. Otherwise, the polygon was an irregular polygon.
7. We measured the dimensionless distance of each of the seven images from the object well, graphically. These dimensionless image distances are D2, D3, D4, D5, D6 and D7, respectively, and were functions of d1 and d2.

2.2 Development of Mathematical Equation

From n = 360/θ -1(Earlougher (1977), seven (7) images were produced due to angle of inclination θ = 45 degrees. The superposition principle was used to aggregate the pressure drop in the object well as follows: Total dimensionless drop in the object well is equal to sum of dimensionless pressure drop in the object and dimensionless pressure drops of each of the seven image wells. That is,

$$p_D = p_{DOw} + \sum_{i=1}^{i=7} p_{DIwi} \quad (1)$$

Using dimensionless pressure drop expressions for an infinite conductivity and uniform flux horizontal well case(Gringarten and Ramey(1973), Ozkan and Raghavan(1990)), the total dimensionless pressure drop in the object well is

$$p_D = -\frac{\propto}{4L_D} Ei\left(-\frac{r_{wD}^2}{4t_D/c_D}\right) + s - \frac{\propto}{4L_D}\left[\sum_{i=1}^{i=7} Ei\left(-\frac{D_{ilw}^2}{4t_D}\right)\right] \quad (2)$$

The corresponding dimensionless pressure derivative was therefore derived as follows:

$$p'_D = t_D \frac{\partial p_D}{\partial t_D} = \frac{\propto}{4L_D} exp\left(-\frac{r_{wD}^2}{4t_D/c_D}\right) + \frac{\propto}{4L_D}\left[\sum_{i=1}^{i=7} exp\left(-\frac{D_{ilw}^2}{4t_D}\right)\right] \quad (3)$$

For different choices of dimensionless object well distances from the top and bottom boundaries, d1 and d2, respectively, every image well dimensionless distance was measured or calculated. Thereafter, Eqs. (2) and (3) was used to compute dimensionless pressure and dimensionless pressure derivatives, respectively, for varying dimensionless flow times.

3. RESULT AND DISCUSSION

Table 1 shows results of dimensionless pressure and dimensionless pressure derivatives computed for d1 =0.2 and d2 = 0.28, c_D = 1, L_D =10, s = 0 case.

Table 1: *p_D and p_D' for d1 =0.2 and d2 = 0.28,* c_D = 1, L_D =10, s = 0

t_D	$\mathbf{p_D}$	$\mathbf{p'_D}$
10^{-2}	0.513	0.075
10^{-1}	0.847	0.244
1	1.605	0.377
10	2.5	0.397

10^2	3.418	0.399
10^3	4.339	0.4
10^4	5.26	0.4
10^5	6.18	0.4
10^6	7.1	0.4
10^7	8.02	0.4

Figure 2 is a semilog plot of p_{DoT} and $p_{D'oT}$ against t_D.for D1 = 0.2 and D2 = 0.28, c_D = 1, s = 0.

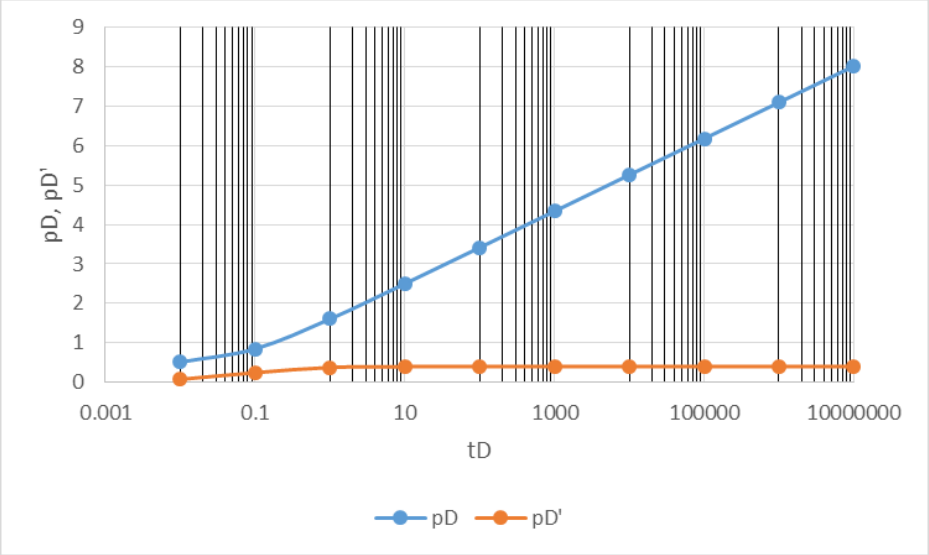

Figure 2: *Plot of p_D and p_D' for D1 =0.2 and D2 = 0.28, cD=1, s = 0*

Tables 2 and 3 show results for different wellbore skins assumed while keeping other already assumed parameters constant. Figure 3 is a semilog plot of p_D and p_D' against t_D of results in Tables 2 and 3.

Table 2: *p_D for D1 =0.2 and D2 = 0.28, cD=1 and Variable Wellbore Skin*

t_D	p_D (s=0)	p_D (s=1)	p_D (s=2)	p_D (s=3)	p_D (s=4)	p_D (s=5)	p_D (s=6)	p_D (s=7)
10^{-2}	0.513	1.513	2.513	3.513	4.513	5.513	6.513	7.513
10^{-1}	0.847	1.847	2.847	3.847	4.847	5.847	6.847	7.847
1	1.605	2.605	3.605	4.605	5.605	6.605	7.605	8.605
10	2.500	3.500	4.500	5.500	6.500	7.500	8.500	9.500
10^2	3.418	4.418	5.418	6.418	7.418	8.418	9.418	10.418
10^3	4.339	5.339	6.339	7.339	8.339	9.339	10.339	11.339
10^4	5.260	6.260	7.260	8.260	9.260	10.160	11.260	12.260
10^5	6.180	7.180	8.180	9.180	10.180	11.180	12.180	13.180
10^6	7.100	8.100	9.100	10.100	11.100	12.100	13.100	14.100
10^7	8.020	9.020	10.020	11.020	12.020	13.020	14.020	15.020

Tables 4 and 5 show results of p_D and p_D' against t_D for varying wellbore skin and wellbore storage, respectively.

Table 3: *p_D' for D1 =0.2 and D2 = 0.28, cD=1 and Variable Wellbore Skin*

t_D	**p_D' (s=0)**	**p_D' (s=1)**	**p_D' (s=2)**	**p_D' (s=3)**
10^{-2}	0.075	0.075	0.075	0.075
10^{-1}	0.244	0.244	0.244	0.244
1	0.377	0.377	0.377	0.377
10	0.397	0.397	0.397	0.397
10^2	0.399	0.399	0.399	0.399
10^3	0.400	0.400	0.400	0.400
10^4	0.400	0.400	0.400	0.400
10^5	0.400	0.400	0.400	0.400
10^6	0.400	0.400	0.400	0.400
10^7	0.400	0.400	0.400	0.400

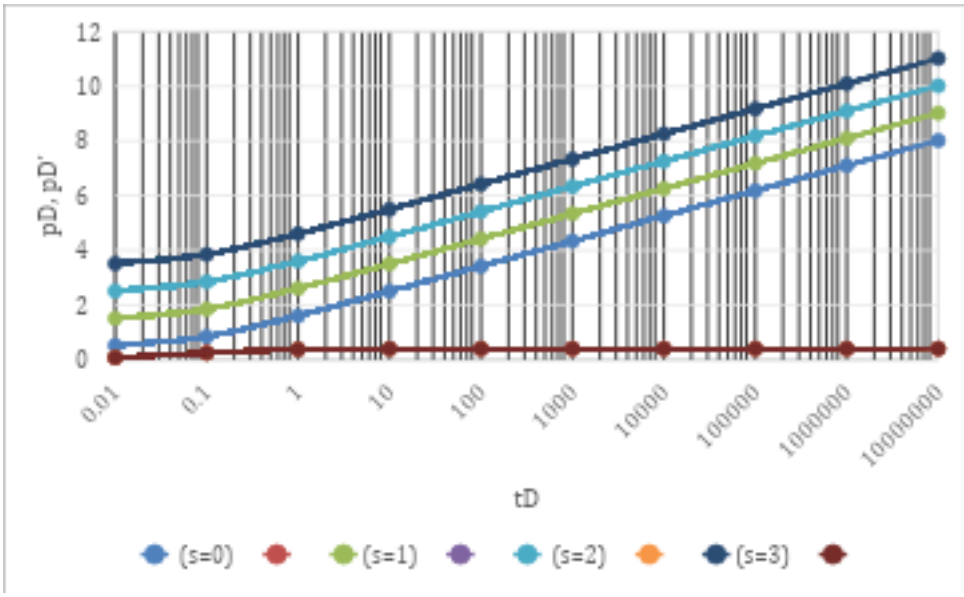

Figure 3: *Plot of p_D and p_D' against t_D of results in Tables 2 and 3*

Table 4: *Results of p_D against t_D for varying and wellbore storage*

t_D	p_D (c_D =1)	p_D (c_D=10)	p_D (c_D=10^2)	p_D (c_D=10^3)	p_D (c_D=5x10^3)	p_D (c_D=10^4)	p_D (c_D=5x10^4)	p_D (c_D=10^5)
10^{-2}	0.513	0.4	0.284	0.169	0.094	0.065	0.02	0.015
10^{-1}	0.847	0.731	0.617	0.502	0.422	0.388	0.312	0.283
1	1.605	1.491	1.379	1.26	1.18	1.145	1.065	1.032
10	2.50	2.388	2.273	2.157	2.077	2.042	1.962	1.928
10^2	3.418	3.303	3.188	3.073	2.922	2.958	2.876	2.843
10^3	4.339	4.223	4.108	3.993	3.914	3.879	3.798	3.763
10^4	5.260	5.145	5.030	4.915	4.835	4.800	4.720	4.685
10^5	6.180	6.065	5.950	5.835	5.755	5.720	5.640	5.600

Table 5: *Results of $p_{D'oT}$ against t_D for varying and wellbore storage*

t_D	p_D' $c_D=1$	p_D' $c_D=10$	p_D' $c_D=10^2$	p_D' $c_D=10^3$	p_D' $c_D=5x10^3$	p_D' $c_D=10^3$	p_D' $c_D=5x10^4$	p_D' $c_D=10^5$
10^{-2}	0.075	0.075	0.075	0.075	0.075	0.075	0.075	0.075
10^{-1}	0.244	0.244	0.244	0.244	0.244	0.244	0.244	0.244
1	0.377	0.377	0.377	0.377	0.377	0.377	0.377	0.377
10	0.397	0.397	0.397	0.397	0.397	0.397	0.397	0.397
10^2	0.399	0.399	0.399	0.399	0.399	0.399	0.399	0.399
10^3	0.400	0.400	0.400	0.400	0.400	0.400	0.400	0.400
10^4	0.400	0.400	0.400	0.400	0.400	0.400	0.400	0.400
10^5	0.400	0.400	0.400	0.400	0.400	0.400	0.400	0.400
10^6	0.400	0.400	0.400	0.400	0.400	0.400	0.400	0.400
10^7	0.400	0.400	0.400	0.400	0.400	0.400	0.400	0.400

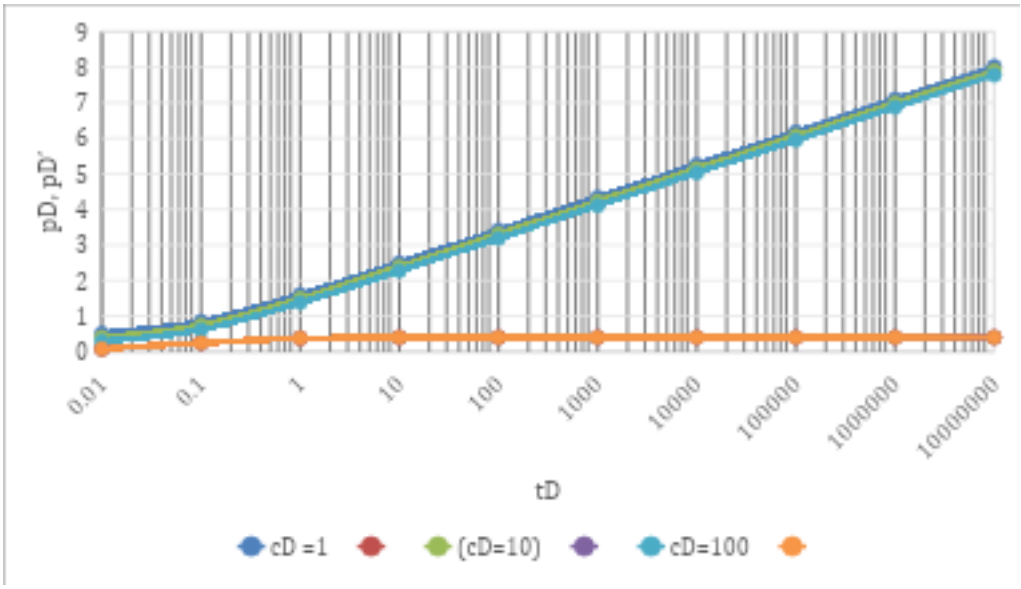

Figure 4: *Results of p_D and p_D' against t_D for varying and wellbore storage*

For varying dimensionless well radii, Tables 6, 7 and Figure 5 show results of p_D and p_D' for selected well parameters above against t_D.

Tables 6: *Results of p_D for selected well parameters against t_D*

t_D	p_D (r_{wD}= 0.001)	p_D (r_{wD}= 0.001)	p_D (r_{wD}= 0.002)	p_D (r_{wD}= 0.003)	p_D (r_{wD}= 0.005)	p_D (r_{wD}= 0.01)	p_D r_{wD}= (0.02)	p_D (r_{wD}= 0.03)
10^{-2}	0.744	0.513	0.445	0.404	0.353	0.284	0.215	0.175
10^{-1}	1.077	0.847	0.778	0.737	0.686	0.617	0.547	0.508
1	1.835	1.605	1.536	1.495	1.444	1.375	1.306	1.265
10	2.722	2.5	2.434	2.393	2.342	2.273	2.204	2.163
10^2	3.648	3.418	3.350	3.308	3.259	3.188	3.119	3.078
10^3	4.569	4.339	4.27	4.229	4.178	4.100	4.039	3.998
10^4	5.491	5.260	5.142	5.150	5.099	5.030	4.961	4.920
10^5	6.411	6.180	6.112	6.014	6.019	5.950	5.881	5.841
10^6	7.333	7.1	7.034	6.993	6.942	6.872	6.803	6.763
10^7	8.250	8.020	7.954	7.910	7.862	7.792	7.724	7.683

Tables 7: *Results of $p_{D'}$ for selected well parameters against t_D*

t_D	$p_{D'}$ (r_{wD}= 0.001)	$p_{D'}$ (r_{wD}= 0.001)	$p_{D'}$ (r_{wD}= 0.002)	$p_{D'}$ (r_{wD}= 0.003)	$p_{D'}$ (r_{wD}= 0.005)	$p_{D'}$ (r_{wD}= 0.01)	$p_{D'}$ r_{wD}= (0.02)	$p_{D'}$ (r_{wD}= 0.03)
10^{-2}	0.075	0.075	0.075	0.075	0.075	0.075	0.075	0.075
10^{-1}	0.244	0.244	0.244	0.244	0.244	0.244	0.244	0.244
1	0.377	0.377	0.377	0.377	0.377	0.377	0.377	0.377
10	0.397	0.397	0.397	0.397	0.397	0.397	0.397	0.397
10^2	0.399	0.399	0.399	0.399	0.399	0.399	0.399	0.399
10^3	0.400	0.400	0.400	0.400	0.400	0.400	0.400	0.400
10^4	0.400	0.400	0.400	0.400	0.400	0.400	0.400	0.400
10^5	0.400	0.400	0.400	0.400	0.400	0.400	0.400	0.400
10^6	0.400	0.400	0.400	0.400	0.400	0.400	0.400	0.400
10^7	0.400	0.400	0.400	0.400	0.400	0.400	0.400	0.400

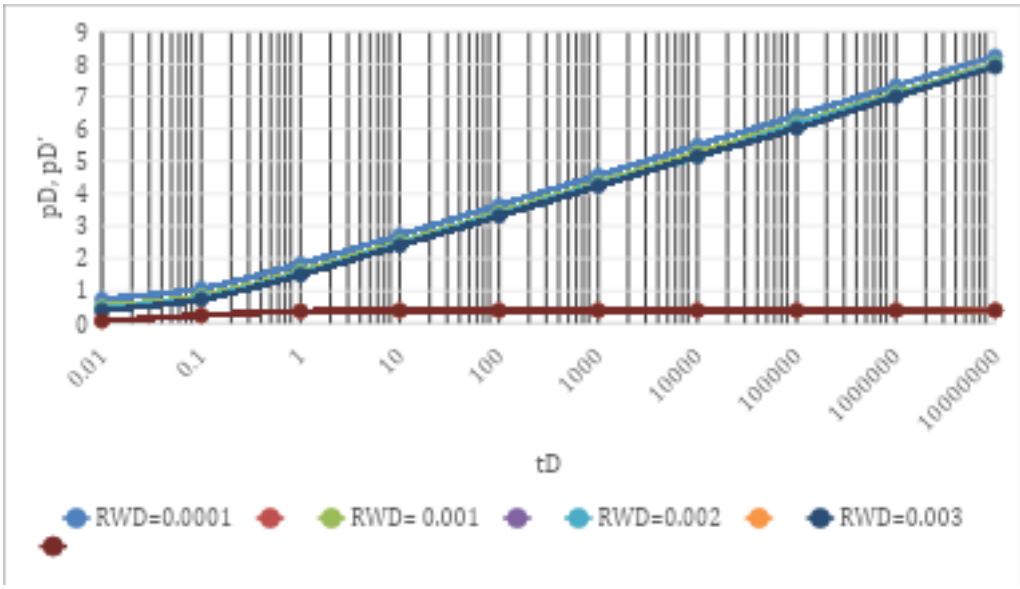

Figure 5: *Results of p_D for selected well parameters against t_D*

For varying L_D, computed p_D and p_D' are tabulated in Tables 8 and 9.

Table 8: *p_D for varying L_D for selected parameters against t_D*

tD	L_D=10	L_D= 100	L_D= 200	L_D= 300	L_D= 500	L_D= 1000	L_D= 2000	L_D= 2500
10^{-2}	0.513	0.051	0.027	0.017	0.01	0.005	0.003	0.002
10^{-1}	0.847	0.084	0.042	0.028	0.017	0.008	0.004	0.003
1	1.605	0.160	0.080	0.053	0.032	0.016	0.008	0.006
10	2.5	0.25	0.125	0.083	0.05	0.025	0.013	0.01
10^{2}	3.418	0.341	0.17	0.114	0.068	0.034	0.017	0.013
10^{3}	4.339	0.433	0.217	0.145	0.086	0.043	0.022	0.017
10^{4}	5.260	0.526	0.263	0.175	0.105	0.052	0.0263	0.021
10^{5}	6.180	0.618	0.308	0.206	0.123	0.061	0.031	0.024
10^{6}	7.100	0.710	0.354	0.230	0.142	0.071	0.035	0.028
10^{7}	8.020	0.802	0.400	0.267	0.160	0.080	0.040	0.032

For a new set of object and image dimensionless distances D1 = 2, D2 = 2.8, D3 = 7.1, D4 = 7.1, D5 = 5.1, D6 = 4.9, and D7 = 5.6, Tables 10 to 17 show results of dimensionless pressure and dimensionless pressure derivatives computed.

Table 9: *p_D' for varying L_D for selected parameters against t_D*

tD	P_D' (L_D= 10)	P_D' (L_D= 100)	P_D' (L_D= 200)	P_D' (L_D= 300)	P_D' (L_D= 500)	P_D' (L_D= 1000)	P_D' (L_D= 2000)	P_D' (L_D= 2500)
10^{-2}	0.075	0.040	0.020	0.013	0.008	0.004	0.002	0.002
10^{-1}	0.244	0.040	0.020	0.013	0.008	0.004	0.002	0.002
1	0.377	0.040	0.020	0.013	0.008	0.004	0.002	0.002
10	0.397	0.040	0.020	0.013	0.008	0.004	0.002	0.002
10^2	0.399	0.040	0.020	0.013	0.008	0.004	0.002	0.002
10^3	0.400	0.040	0.020	0.013	0.008	0.004	0.002	0.002
10^4	0.400	0.040	0.020	0.013	0.008	0.004	0.002	0.002
10^5	0.400	0.040	0.020	0.013	0.008	0.004	0.002	0.002
10^6	0.400	0.040	0.020	0.013	0.008	0.004	0.002	0.002
10^7	0.400	0.040	0.020	0.013	0.008	0.004	0.002	0.002

Table 10: *p_D and p_D' for s = 0, D1 = 2 and D2 = 2.8, L_D= 1*

t_D	**p_D (s=0)**	**p'_D (s=0)**
0.01	0.2702	0.041
0.1	0.3858	0.3894
1	0.5145	0.7442
10	0.8430	2.4093
10^2	1.5891	3.7684
10^3	2.4902	3.9758
10^4	3.4088	3.9975
10^5	4.3321	3.9997
10^6	5.2500	3.9999
10^7	6.1741	3.9999

Table 11: *p_D and p_D' for s = 1, D1 = 2 and D2 = 2.8, L_D= 1*

t_D	p_D (s=1)	p_D'
0.01	1.2702	0.041
0.1	1.3858	0.3894
1	1.5145	0.7442
10	1.843	2.4093
100	2.5891	3.7684
1000	3.4902	3.9758
10000	4.4088	3.9975
100000	5.3321	3.9997
1000000	6.25	3.9999
10000000	7.1741	3.9999

Table 12: *p_D and p_D' for c_D = 0, D1 = 2 and D2 = 2.8, L_D= 1*

t_D	p_D (c_D=1)	p_D'
0.01	0.2702	0.041
0.1	0.3858	0.3894
1	0.5145	0.7442
10	0.843	2.4093
100	1.5891	3.7684
1000	2.4902	3.9758
10000	3.4088	3.9975
100000	4.3321	3.9997
1000000	5.25	3.9999
10000000	6.1741	3.9999

Table 13: *p_D and p_D' for c_D = 10, D1 = 2 and D2 = 2.8, L_D= 1*

t_D	p_D (c_D=10)	p_D'
0.01	0.3858	0
0.1	0.5009	0.041
1	0.6296	0.645
10	0.9583	2.3982
100	1.7042	3.7673
1000	2.6053	3.9757
10000	3.5239	3.9975
100000	4.4471	3.9997
1000000	5.5679	3.9999
10000000	6.2896	3.9999

Table 14: p_D and p_D' for L_D = 1, D1 = 2 and D2 = 2.8

t_D	p_D (L_D=10)	p_D'
0.01	0.2702	0.041
0.1	0.3858	0.3894
1	0.5145	0.7442
10	0.843	2.4093
100	1.5891	3.7684
1000	2.4902	3.9758
10000	3.4088	3.9975
100000	4.3321	3.9997
1000000	5.25	3.9999
10000000	6.1741	3.9999

Table 15: *p_D and p_D' for L_D = 1, D1 = 2 and D2 = 2.8*

t_D	p_D (L_D=100)	p_D'
0.01	0.027	0
0.1	0.0385	0
1	0.0514	0.2975
10	0.0843	2.2999
100	0.1589	3.7562
1000	0.249	3.9746
10000	0.3408	3.9975
100000	0.4332	3.9997
1000000	0.525	3.9999
10000000	0.6174	3.9999

Table 16: *p_D and p_D' for r_{wD} = 0.001, D1 = 2 and D2 = 2.8, L_D= 1*

t_D	p_D (r_{wD} = 0.001)	p_D'
0.01	0.2702	0.041
0.1	0.3858	0.3894
1	0.5145	0.7442
10	0.843	2.4093
100	1.5891	3.7684
1000	2.4902	3.9758
10000	3.4088	3.9975
100000	4.3321	3.9997
1000000	5.25	3.9999
10000000	6.1741	3.9999

Table 17: *p_D and p_D' for r_{wD} = 0.1, D1 = 2 and D2 = 2.8*

t_D	p_D (r_{wD} = 0.1)	p_D'
0.01	0.0522	0
0.1	0.1568	00
1	0.2842	0.2975
10	0.6127	2.2999
100	1.3588	3.7562
1000	2.2599	3.9746
10000	3.1785	3.9975
100000	4.1019	3.9997
1000000	5.0228	3.9999
10000000	5.9441	3.9999

In the early stages, the graphs indicate a wellbore storage-dominated phase, as seen by the high slope in the derivative as shown in results of Tables 1 to 9, and Figures 2 to 7. This reflects that fluid accumulation within the wellbore dominated over reservoir flow, typical in horizontal wells. As time progressed, the influence of the wellbore storage in Tables 4 diminished, transitioning into bilinear flow. Here, p_D and p_D' illustrated a distinct slope, influenced by the 45° inclination of the boundaries. The bilinear flow reflected interaction between the reservoir and the boundaries, with the angle influencing lateral flow towards the well. The p_D and p_D' curves in Figures 2 to 5 subsequently entered a phase where the flow behavior aligned with linear and pseudo-radial flow regimes. The pseudo-radial flow was marked by a stable p_D curve, indicating that flow was well-established along the inclined boundaries. Notably, the 45° inclination appeared to delay the onset of pseudo-radial flow, showing the effect of boundary orientation on flow convergence. At larger t_D values, sealing boundaries impacted the well performance as indicated by the p_D asymptotic and derivative stabilization. The results of Tables 9 to 17 revealed that the pressure derivative flattened as flow converged at the inclined sealing boundary, illustrating limited drainage due to the boundary's restriction. From Table 9, higher drainage length contributed to prolonged initial and transitional flow behaviors, delaying boundary effects, and supported higher productivity. As shown in Tables 4 and 5, lower wellbore storage coefficients reinforced the wellbore storage effect in early-time behavior, causing a steeper initial slope in the p_D' response. This parameter shaped the graph in early stages and highlighted the wellbore's capacity to absorb fluid before the

reservoir flow stabilized. The smaller the dimensionless wellbore radius yielded increased p_D and p_D' for all well designs and flow times as shown in Tables 6 and 7. This parameter had a pronounced effect in the transition from bi-linear to linear flow, where small radius effects amplified derivative fluctuations before stabilizing.

With larger values of wellbore skin, p_D values were reduced due to additional flow restrictions near the wellbore as shown in Table 6. From results in Tables 8 and 14, for the same L_D, dimensionless pressure drop decreased when the object well was farther away from the sealing boundaries, thus indicated acceleration to attainment of pseudosteady state and end of producing well life. Results from all the tables show consistent dimensionless pressure gradient(per cycle) and dimensionless pressure derivative of $9.2104/L_D$ and $4/L_D$, respectively.

4. CONCLUSION

Dimensionless pressures and dimensionless pressure derivatives of a horizontal well within sealing boundaries at 45° inclination have been computed over varying dimensionless flow times. There were seven (7) image wells generated due to the inclination. Dimensionless pressure gradients and derivatives of $9.2104/L_D$ and $4/L_D$, respectively, characterized flow at large dimensionless flow times. Higher dimensionless well length prolonged the pseudo-linear flow regime, and delayed boundary-dominated flow. Larger dimensionless well radius increased early-time pressure gradients. High skin factors and wellbore storage caused increased pressure drop and delayed response of transients by the inclined reservoir external boundaries. The farther the object well was from the external boundaries, the longer the well experienced infinite-acting flow, and therefore, delayed pseudo steady state flow.

CONFLICT OF INTEREST

No conflict of interest was declared by the authors.

REFERENCES

[1] Al Rbeawi, S. and Tiab, D. (2013). Transient Pressure Analysis of Horizontal Wells in a Multi-Boundary System ,*American Journal of Engineering Research*, 2(4), 44 - 66.

[2] Babu, D.K and Odeh, A.S. (1990) Transient Flow Behavior of Horizontal Wells; Pressure Drawdown and Buildup Analysis. *SPE Formation Evaluation* , 7-15.

[3] Carslaw, H.S. Jaeger, J.C.(1959). *Conduction of Heat Through Solids*. 2nd Ed. Oxford University Press, London, England, 258.

[4] Daviau, F. Mouronval, G. Bourdarot, G. and Curutchet, P.(1988). Pressure Analysis for Horizontal Wells, *SPERE*, 716 - 724, *Trans*., AIME, 285.

[5] Earlougher, R.C.Jr. (1977) *Advances in Well Test Analysis*,SPE Monograph Series, (5), 124.

[6] Escobar F. H, Muñoz O. F and Sepúlveda J. A (2004) Horizontal Permeability Determination From The Elliptical Flow Regime of Horizontal Wells. CT&F - *Ciencia, Tecnología y Futuro*, 2(5), 83 - 95.

[7] Galas, C.M.F., Churcher, P.L. and Tottrup, P. (1994). Prediction of Horizontal Well Performance in a Mature Waterflood, Weyburn Unit, Southeasthern Saskatchewan, *J. of Canadian Petroleum Techology*, 33(9). Paper No. PETSOC-94-09-03.

[8] Gringarten, A. and Ramey, H. J. (1973) The Use of Source and Green's Functions in Solving Unsteady-Flow Problems in Reservoirs; *SPEJ*, October, 285 – 296.

[9] Matthews, C.S. and Russell, D.G. (1967). *Pressure Buildup and Flow Tests in Wells*, Monograph Series, SPE of AIME, 1.

[10] Kuchuk, F.J. (1995). Well Testing and Interpretation for Horizontal Wells. *J Pet Technology* 47 (1), 36 - 41.

[11] Ozkan, E. and Raghavan, R. (1990). Performance of Horizontal Wells Subject to Bottom Water Drive, *SPE Reservoir Engineering*, AIME *Trans*., 375 – 383.

[12] Odeh, A.S. and Babu, D.K. (1990). Transient Flow Behavior of Horizontal Wells: Pressure Drawdown and Buildup Analysis. *SPE Form Eval* 5(1): 7-15. SPE-18802-PA. http://dx.doi.org/10.2118/18802-PA.

APPENDIX

Nomenclature

d1 Dimensionless object well distance from upper sealing boundary

d2 Dimensionless object well distance from lower sealing boundary

D_i Dimensionless image distance i = 1, 2, 3, 4, 5,6 ,7

Ei Exponential integral function

p_D Dimensionless pressure

p_D' Pressure derivative

p_D Total dimensionless pressure in the object well

$p_{,D}$ Total dimensionless pressure derivative in the object well

L_D Dimensionless well length

r_{wD} Dimensionless well radius

c_D Dimensionless well storage coefficient

s Skin factor

t_D Dimensionless time